International Journal of Non-Linear Mechanics 132 (2021) 103710

Contents lists available at ScienceDirect

International Journal of Non-Linear Mechanics

journal homepage: www.elsevier.com/locate/nlm

Computational corroboration of the flow of rock glaciers against borehole measurements

Krishna Kannan [a], Daniela Mansutti [b,*], Kumbakonam R. Rajagopal [c]

[a] Department of Mechanical Engineering, Indian Institute of Technology Madras, Chennai 600 036, India
[b] Istituto per le Applicazioni del Calcolo 'M. Picone', CNR - Rome, via dei Taurini, 19, Italy
[c] Department of Mechanical Engineering, Texas A&M University, College Station, TX 77845, USA

ARTICLE INFO

Keywords:
Ice
Rock and sand grains
Constitutive law
Rock glacier
Murtel-Corvatsch alpine glacier
Deformations

ABSTRACT

In this study, we computationally corroborate the flow of rock glaciers against borehole measurements, within the context of a model previously developed (2020). The model is, here, tested against the simulation of the sliding motion of the Murtel-Corvatsch alpine glacier, which is characterized in detail in the literature with internal structure description and borehole deformations measurement.

The capability of the model to take into account the composition of the rock glacier, as a mixture of ice and rock and sand grains with the local impact of pressure and heat transfer, results in the accurate detection of the internal sliding.

With careful calibration of the model parameters, the computed numerical solution of the model reports a relative error of 1.8% and of 0.3% in the reproduction of the measured shear zone velocity and of the ratio of measured shear zone deformation over top surface deformation, respectively.

Furthermore a deeper understanding of the role of the model parameters involved in the simulation of such a process is also gained and we discuss the same in detail.

1. Introduction of the model

In a previous paper [1] the authors developed a mathematical model for the flow of a rock glacier which takes into consideration thermal effects. Here we develop a computational scheme to solve the system of governing equations and solve the same numerically. The solution obtained is corroborated versus observed data on the evolution of the Murtel-Corvatsch alpine rock glacier.

We start by briefly discussing the salient aspects of the development of the governing equations that stem from the balance of mass, and linear momentum. The balance of mass takes the form:

$$\frac{d\,\rho}{dt} + div\,(\rho\mathbf{v}) = 0, \tag{1}$$

while the balance of linear momentum is given by:

$$div\,\mathbf{T}^T + \rho\mathbf{b} = \rho\dot{\mathbf{v}} \tag{2}$$

where ρ is the density of ice, $\mathbf{v}$, the velocity field, $\mathbf{T}$, the Cauchy stress tensor and $\mathbf{b}$, the specific body force. Also the dot denotes the material time derivative.

Most existing works in the literature in computational glaciology adopt Glen's law [2], based on the representation of ice as a dense viscous fluid with

$$\mathbf{T} = -p\mathbf{I} + \mu_G\mathbf{A}_1, \tag{3}$$

where p is the indeterminate part of the stress due to the constrain of incompressibility, $\mathbf{I}$ is the identity tensor, $\mathbf{A}_1$ is twice the symmetric part of the velocity gradient, $\mathbf{A}_1 = \mathbf{L} + (\mathbf{L})^T$ and $\mathbf{L} = grad(\mathbf{v})$, and μ_G is the generalized viscosity having this form:

$$\mu_G = \mu_G(\partial_i v_j) = \mu_0[\frac{1}{2}tr(\mathbf{A}_1^2)]^{\frac{m}{2}} \tag{4}$$

being ∂_i, the partial differential operator along the ith spacial direction, v_j, the jth component of the velocity field (with i and j repeated from 1 to 3), μ_0, a scalar factor of phenomenological character, and m, a scalar parameter. This model, including the strain rate effect onto ice viscosity, represents successfully the secondary creep [3].

The formation of lateral moraines in relation to certain dynamical conditions of the rock glaciers is partially traced back to a typical non-newtonian behavior occurring in rectilinear shearing flow, which is supported by non-zero normal stress differences and qualitatively sums up to a thrust carrying debris along in each direction normal to the shear direction.

As of mathematical modeling, normal stress differences are both non identically zero for differential type fluid models of grade n, with $n > 1$. The Newtonian (Navier–Stokes) fluid model is of differential

* Corresponding author.
E-mail address: d.mansutti@iac.cnr.it (D. Mansutti).

https://doi.org/10.1016/j.ijnonlinmec.2021.103710
Received 26 January 2021; Received in revised form 1 March 2021; Accepted 2 March 2021
Available online 10 March 2021
0020-7462/© 2021 The Author(s). Published by Elsevier Ltd. This is an open access article under the CC BY-NC-ND license (http://creativecommons.org/licenses/by-nc-nd/4.0/).

type with $n = 1$ [4] as well as the mentioned Glen's law for ice, which, consequently, cannot predict the whole process of moraine formation.

McTigue, Passman and Jones [3] modeled the creep of ice by using a second order fluid model (SOFM) the simplest constitutive equation capable of describing both primary and secondary creep, which also includes normal stress differences arising in shearing flow. [1] Along this line Man and Sun in [6] modified SOFM with a Glen-like functional expression of the viscosity coefficient in order to regain the strain rate effects as reflected in Glen's law. The expression of the modified SOFM (MSOFM) stress tensor is

$$\mathbf{T} = -p\mathbf{I} + \mu_G \mathbf{A}_1 + \alpha_1 \mathbf{A}_2 + \alpha_2 \mathbf{A}_1^2, \tag{5}$$

where α_1 and α_2 are material scalar parameters to be fixed and $\mathbf{A_2}$ is the second Rivlin–Ericksen tensor, describing the frame-indifferent time derivative of the velocity gradient tensor, that is

$$\mathbf{A}_2 = \dot{\mathbf{A}}_1 + \mathbf{A}_1\mathbf{L} + \mathbf{L}^T\mathbf{A}_1$$

with $\dot{\mathbf{A}}_1$, the material time derivative of tensor $\mathbf{A}_1$.

It is worth to mention that the MSOFM model has been extended in order to include the effect of pressure as measured by Barrette and Jordaan, who reported in [7] several experimental tests on the mechanical response of ice under compressive load and in presence of confinement pressures. Arcangioli et al. in [8] derived the upgraded model basing on implicit theories of continuum mechanics and obtaining an appropriate choice of the functional expression of the material parameters by matching with the experimental creep curves.

However let us observe that the above listed models are essentially for clean ice. In the case of rock or debris-laden glaciers, the impact of pressure, and also temperature on the viscosity coefficient must be included in relation to the concentration of debris and particle size. Actually, here, within the flow of the glacier, ice melting temperature undergoes local changes due to (non-hydrostatic) pressure increase caused by the interaction of ice with included rock fragments, and subsequent local phase transition events lead to release of water influencing ice–debris mixture viscosity [9]. This behavior has been recently reviewed by Moore in [10] who reconsidered a broad range of field observations, theory and experimental work relevant to the mechanical interactions between ice and rock debris. It is worth mentioning the observations reported by Lawson and Elliott in [11] from experimental strength testing of real glacier ice. They found that, if debris is incorporated, transition from ductile to brittle regime (when crevasses may form) strongly depends on temperature, so that if temperature decreases, critical total strain also decreases, meanwhile compressive strength of rock glacier ice increases to its maximum as effect of regelation of previously formed water films, hardening around rocky particles. The mechanism shaping ice–debris mixtures constitutive behavior is summarized by Moore [10] as a "competition between the role of debris in impeding ice creeping" (as for 'locking' in the case of granular material) "and the mitigating effect of unfrozen water at debris–ice interface", driven by shear rate, pressure, temperature, salinity, debris concentration and particle size.

In 2013 two of the authors, Kannan and Rajagopal, proposed a generalization of the Man and Sun's constitutive equation (5) in order to describe, at the mechanical level, the impact of debris trapped in ice [12]. Recently, in 2020 present authors published an extension of that model including explicitly also the representation of the thermal field [1]. These upgrades are obtained with an appropriate choice of the viscosity coefficient and of the normal stress parameters as functions depending also on pressure, temperature and solid fraction. Inspiration is taken from the work on dense suspensions of a newtonian fluid and hard spherical particles by Mills and Snabre [13] regarding the functional expression of the viscosity coefficient, and from the work on non-colloidal suspensions of a non-newtonian fluid and hard spherical particles by Morris and Boulay [14] regarding the normal stress parameters. For the dependency of the three parameters on the temperature field, an Arrhenius type behavior is adopted ensuing on-field observation data [15].

Without going into the details that can be found in the mentioned publications, we recall the main formulas and equations of the extended model in [1] which is, here, the object of validation.

In particular let us rewrite, first, the Cauchy stress tensor with renamed coefficients:

$$\mathbf{T} = -p\mathbf{I} + \mu_{KMR}\mathbf{A}_1 + \alpha_{KMR,1}\mathbf{A}_2 + \alpha_{KMR,2}\mathbf{A}_1^2, \tag{6}$$

having the form:

$$\mu_{KMR} = \mu_{KMR}(\partial_i v_j, \hat{p}, T) =$$

$$\mu_G(\partial_i v_j)\left[(1-f)\left(1 + k_1\sqrt{\frac{\hat{p}-P_a}{P_a}}\right) + f k_2\,\frac{\hat{p}-P_a}{P_a}\right]\cdot e^{B(\frac{1}{T}-\frac{1}{T_0})} \tag{7}$$

$$\alpha_{KMR,i} = \alpha_{KMR,i}(T) =$$

$$\alpha_i^0\left[1 + k_{i+2}\frac{\bar{\phi}^2}{(1-\bar{\phi})^2}\right]\cdot e^{B_i(\frac{1}{T}-\frac{1}{T_0})}, \quad i = 1,2 \tag{8}$$

where $\hat{p} = -\frac{1}{3}\,tr(\mathbf{T})$ is the negative of the mean normal stress, T is the temperature, μ_G is the Glen's viscosity coefficient in (4), f and $\bar{\phi}$ are the equilibrium solid fraction and the relative solid fraction of rock and sand grains trapped in the ice interstices, respectively, α_i^0 and k_i for $i = 1,..,4$ are material constants, B and B_i are activation constant factors, P_a is the atmospheric pressure and T_0 is the transition temperature of the material property. Taking into account the thermodynamical arguments of Dunn and Fosdick [16] and the results of Man and Sun in [6], as extensively explained in [12], the relation $\alpha_{KMR,1} + \alpha_{KMR,2} = 0$ has to be met.

The definition of f and $\bar{\phi}$ requires the introduction of the solid fraction of rock and sand grains trapped within the ice interstices, called ϕ, and of the maximum solid fraction of such particles achievable in the 'random-close-packing configuration' (the reader is referred to granular materials terminology), denoted by ϕ_{max}. Then we can introduce:

$$\bar{\phi} = \frac{\phi}{\phi_{max}}, \tag{9}$$

$$\mathrm{f} = \frac{\bar{\phi}}{\bar{\phi} + \mathrm{e}(1-\bar{\phi})}, \tag{10}$$

with e measuring the extent of sliding effect due to the presence of water film at the surface of the 'free-to-move' rock particles, whose relative fraction is quantified by $(1-\bar{\phi})$. It is worth noting that f is close to 1, its maximum value, either when e is null or when $\phi = \phi_{max}$, that is either in condition of null sliding effect of the 'free-to-move' solid particles or when solid particles are so densely distributed to prevent any motion. On the contrary, the value of f decreases along with increasing values of e and/or increasing values of $(1-\bar{\phi})$, both conditions corresponding to increasing mobility of the 'free-to-move' solid particles either due to the presence of more water film with lubricating effect at their interface with ice or for being surrounded by pure ice and, so, flowing as a part of it without offering any additional resistance. Compared to $\bar{\phi}$, the equilibrium solid fraction, f, represents also the impact of ice or water around the solid particles and distinguishes the possibility that solid particles move and subtract themselves from the set of the fixed ones and join the dynamics of ice, so inducing shear-thinning within ice flow (f decreasing), from the possibility that they keep themselves locked with each other inside ice interstices ($f = 1$). The numerical tests, that will be presented and discussed later, show undoubtedly the critical role played by these quantities in the detection and characterization of sliding occurring in rock glacier flow.

The structure of this paper is the following: in Section 2, the test case and its mathematical formulation are described; in Section 3, the numerical solution approach and the numerical results are presented and discussed versus the model validation purpose. In Section 4 conclusions and future work perspective are drawn.

[1] There has been a great deal on unnecessary controversy concerning the status of these models. A critical review and a detailed discussion of the same have been developed by Dunn and Rajagopal in [5].

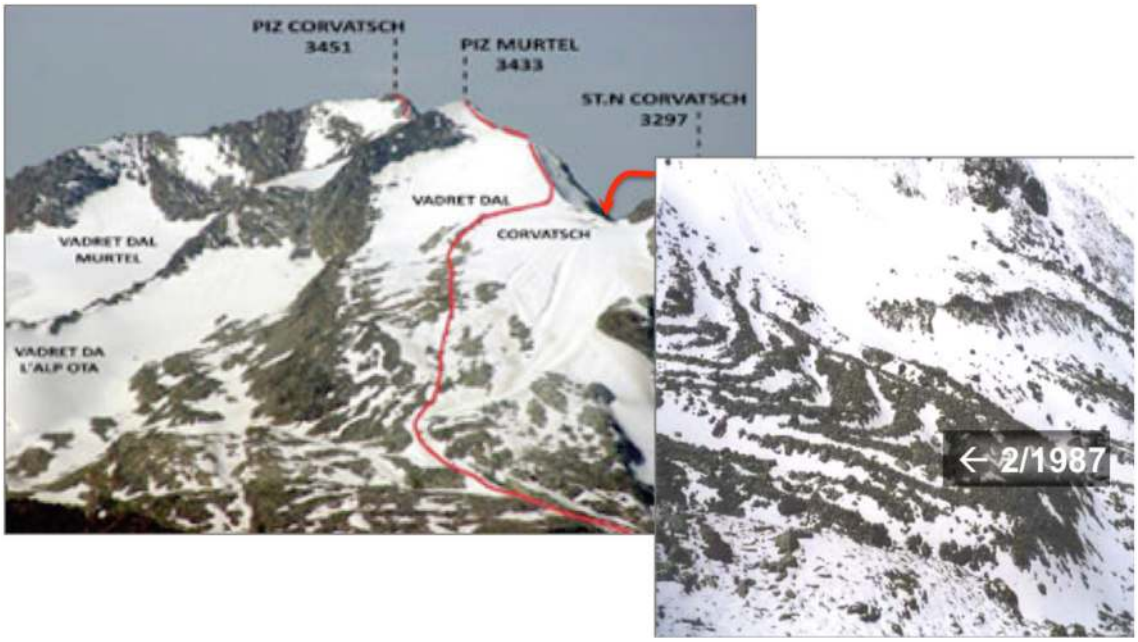

Fig. 1. Murtel Corvatsch alpine rock glacier in the Upper Engadin, Switzerland, with the location of the borehole 2/1987.

2. The test case

The constitutive character of rock glaciers makes them possibly very unstable as effective viscosity can reach up to seven times smaller than for clean ice with consequent onset of shear flow. When shear flow establishes, it may be rigid and fast with possible devastating effects. For the criticality of this situation we have decided to challenge the KMR model with regard to the detection of the shear zone of a rock-glacier flow very well documented in the literature, as it is in the case of Murtel-Corvatsch glacier in the Upper Engadin, Switzerland, shown in Fig. 1.

2.1. Natural set-up and its representation

In [17], based on borehole measurements, Arenson et al. pointed out that, in contrast to temperate glaciers, permafrost within rock glaciers has distinct shear zones where deformations concentrate. And also they observed that the flow velocity depends on the temperature and the composition. Actually, the KMR model covers both of the aspects. Furthermore, they provided the measurement of deformation and temperature in depth in several boreholes combined with a sufficiently detailed description of the local composition of the glacier making their set-up particularly suitable to our aim.

We have focused on the borehole 2/1987 (whose location is highlighted in Fig. 1) and from the corresponding data and qualitative picture, we have reconstructed the profile of $\bar{\phi}$ as in the plot in Fig. 2, where it is also shown that, h, the thickness of the glacier, is about $60m$. Let us observe that $\bar{\phi}$ has a value very close to 1 in the lower layer, identified as 'essentially' rocky zone, and a value smaller than 0.2 in the upper layer, which is an 'essentially' icy zone, whereas, in the internal 3 m thick layer at a distance of 28.4 from bedrock, the value decreases linearly towards the upper layer. It is expected that here, being the glacier neither rigid rock nor temperate, the peculiarities of the behavior of the rock-glacier might be enhanced. As suggested also in the paper [12], we have fixed $\phi_{max} = 0.605$, following the observations of Ovralez et al. who studied a dense suspension of non colloidal particles via magnetic resonance imaging [18]. The corresponding value of e and, consequently, the graph of f (the last one also plotted in Fig. 2), have been fixed according to the results of a series of numerical trials finalized to shoot the measured deformation profile (this aspect will be extensively discussed in Section 3.2); such testing lead us to fix $e = 175$ at the 'essentially' rocky zone and at the zone of ice 'averagely' mixtured with sand and rocky grains, and $e = 1.1$ in the 'essentially' icy zone. As suggested by the functional expression of f, the impact of a value of e is related to the corresponding value of the quantity $(1 - \bar{\phi})$ and it is quite different if such a quantity approaches 1 rather than being almost null.

Another important information for the present validation procedure is the in-depth temperature profile that we have obtained from Arenson et al. data and picture. At borehole 2/1987 the reconstructed sketch of temperature in the time period 1987–1990 is shown in Fig. 3. In their paper Arenson et al. commented that, in the following time period 1991–1995, an increase of 0.5 °C was perceived at the shear zone in [28.4 m, 31.4 m]. So we have included this information by adjusting correspondingly the previous profile and obtained the temperature plot for the time range 1991–1995 (see Fig. 3).

The surface of Murtel-Corvatsch glacier is characterized by a slope of $\alpha = 14°$, so gravity is an external effective cause of the observed sliding motion. In absence of additional geometrical details, surface slope and glacier thickness are assumed constant in the sliding direction.

Based on the described set up, the validation test consisted in the numerical reproduction of the in-depth borehole deformation profile (shear zone included) at each time shot measured and documented by Arenson et al.

2.2. Governing equations

The geometrical characteristics and the position of the borehole 2/1987, very close to the longitudinal symmetry axis of the glacier and where the ice flow is presumably fully developed, have allowed to adopt the unidirectional approximation. Then, avoiding redundant indicial notation and fixed a reference frame, as in Fig. 4, with origin at the bedrock, (x), horizontal axis parallel to the sliding direction, and (y), vertical axis directed upwards, the unknown velocity and pressure fields assume the form

$$\mathbf{v} = (u(y),\ 0,\ 0)^T \tag{11}$$

$$p = p(y). \tag{12}$$

The particular observed thermal conditions define the test problem as a steady isothermal glacier creeping flow problem, in correspondence

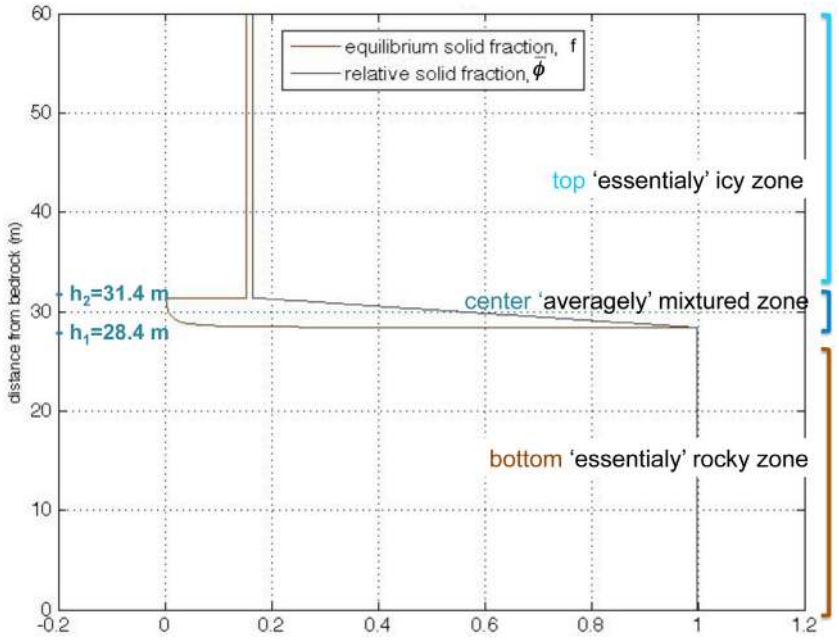

Fig. 2. Relative rock and sand grain fraction and equilibrium solid fraction reconstructed from borehole 2/1987 data in [17].

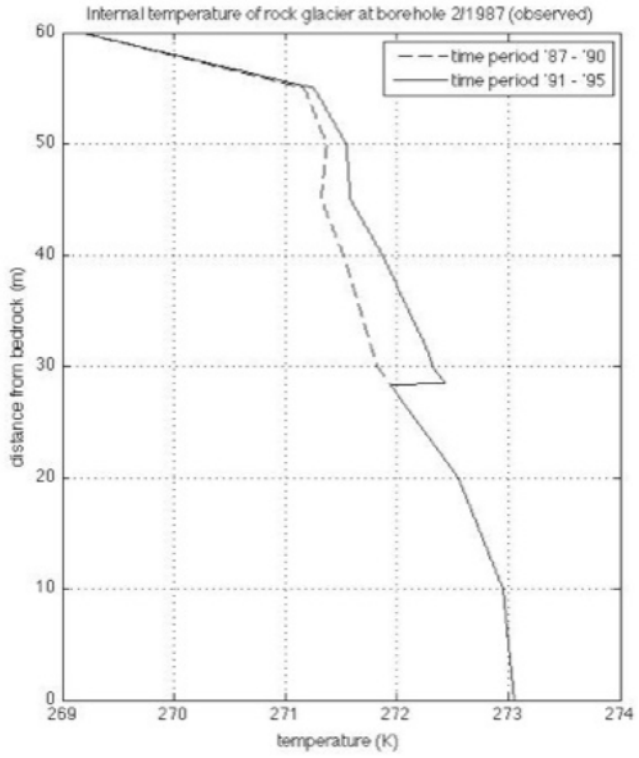

Fig. 3. Measured temperature profile at borehole 2/1987 as in [17].

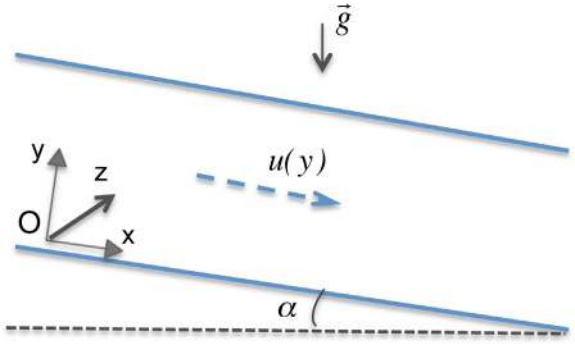

Fig. 4. Geometrical set-up of the test case.

of each measured temperature profile in Fig. 3. The balance of linear momentum reduces to

$$\frac{d}{dy}\left(\mu_{KMR}\, u'\right) = -\rho_{mix}\; g\; sin\alpha \tag{13}$$

$$\frac{d}{dy}\left(-p + \alpha_{KMR,1}\left(u'\right)^2\right) = \rho_{mix}\; g\; cos\alpha, \tag{14}$$

holding for $y \in (0,\ h)$ (u' denotes the first derivative of u). We observe that, being unidirectional, the velocity field meets a priori the incompressibility constrain, $div\ \mathbf{v} = 0$, and it results $\hat{p} = p$.

As μ_{KMR} depends on u', in order to characterize the system let us introduce explicitly its expression, where the value $m = -2/3$ is adopted along with the results in the literature of the classical Glen's law ([15]. Then Eq. (13) becomes

$$\frac{d}{dy}\left(\mu_0\left[(1-f)\left(1 + k_1\sqrt{\frac{p-P_a}{P_a}}\right) + f k_2\,\frac{p-P_a}{P_a}\right]\cdot e^{B\left(\frac{1}{T}-\frac{1}{T_0}\right)}\left(u'\right)^{1/3}\right) = -\rho_{mix}\; g\; sin\alpha \tag{15}$$

Eqs. (14) and (15) represent a second order system of Ordinary Differential Equations (ODE) in $(u,\ p)$ that is determined, here, under the following boundary conditions:

$$u(0) = 0, \tag{16}$$

$$u'(h) = 0,\ p(h) = P_a \tag{17}$$

which describe the no-slip condition at the bedrock, typical for ice below melting temperature, and the dynamical equilibrium between ice and atmosphere at the interface, respectively.

3. Numerical validation of the model

3.1. Numerical solution approach

The first step taken in the solution of the above system is the analytic integration in the generic sub-domain $[y, h]$ (for $y > 0$) which allows to meet the boundary values (17). This operation leads to the system:

$$\mu_0 \left[(1-f)\left(1+k_1\sqrt{\frac{p-P_a}{P_a}}\right)+fk_2\,\frac{p-P_a}{P_a}\right]\cdot e^{B\left(\frac{1}{T}-\frac{1}{T_0}\right)}\left(u'\right)^{1/3} = M\ g\ sin\alpha \tag{18}$$

$$p = P_a+\alpha_{KMR,1}\left(u'\right)^2+M\ g\ cos\alpha \tag{19}$$

being $M = M(y) = \int_y^h \rho_{mix}\,d\bar{y}$, the mass of the layer of rock glacier confined in $[y,\ h]$. This system holds for $y \in (0,\ h]$. Then, by substituting the expression of p as a function of u', (19), into Eq. (18), a first order non-linear ODE is obtained which is rewritten in order to provide the problem with a structure suitable for a following fixed point solution approach. The resulting equation is:

$$u' = (M\ g\ sin\alpha)^3\cdot\left\{\mu_0\left[(1-f)\left(1+k_1\sqrt{\frac{\alpha_{KMR,1}\left(u'\right)^2+M\ g\ cos\alpha}{P_a}}\right)+ fk_2\,\frac{\alpha_{KMR,1}\left(u'\right)^2+M\ g\ cos\alpha}{P_a}\right]\cdot e^{B\left(\frac{1}{T}-\frac{1}{T_0}\right)}\right\}^{-3} \tag{20}$$

that is numerically solved under the remaining boundary condition (16). At this juncture, we discretize the interval domain $[0, h]$ into n uniform subintervals of width $dy = h/n$ and approximate the derivative, u', with the second order centered finite difference scheme. Then, by evaluating the above ODE at the mid-point of each subinterval, $y_{i-1/2} = (i-1/2)\cdot dy,\ i = 1, \ldots, n$, a system of algebraic equations is obtained for $u_i = u(y_i),\ i = 1, \ldots, n$, the numerical velocity of the studied rock glacier. Below the fixed point iteration law adopted for solving the system is shown:

$$u_i^{(k+1)} = u_{i-1}+dy\cdot(M_i\ g\ sin\alpha)^3\cdot \left\{\mu_0\cdot\left[(1-f_i)\left(1+k_1\sqrt{\frac{(\alpha_{KMR,1})_i\left(\frac{u_i^{(k)}-u_{i-1}}{dy}\right)^2+M_i\ g\ cos\alpha}{P_a}}\right)+ f_ik_2\,\frac{(\alpha_{KMR,1})_i\left(\frac{u_i^{(k)}-u_{i-1}}{dy}\right)^2+M_i\ g\ cos\alpha}{P_a}\right]\cdot e^{B\left(\frac{1}{T_i}-\frac{1}{T_0}\right)}\right\}^{-3} \tag{21}$$

with M_i, f_i, $(\alpha_{KMR,1})_i$ and T_i assigned at the mid-point $y_{i-1/2}$. As Eq. (20) is of first order, a straightforward upwards marching procedure has been allowed starting by computing the solution, u_i, from the bedrock where $y_i = y_1 = dy$ and the boundary condition (16) provides the value $u_{i-1} = u_0 = 0$. At each altitude, y_i, the fixed point iterations have been initialized with an approximate value of the glacier velocity, $u_i^{(0)}$, deduced from the local measured deformations reported by Arenson et al. [17] over the elapsed time from the observation starting, 15-9-1987. In the numerical simulations that will be presented in the following sections, iterations have been repeated up to reach a residual $O(10^{-14})$ (equal to relative residual $O(10^{-3})$), in most cases three steps were required.

A posteriori it has been verified that the iteration function is a contraction around the sought numerical solution, which guarantees the convergence of the iterative procedure.

3.2. Parameter calibration and sensitivity analysis

The first step in the numerical simulation of the Murtel-Corvatsch glacier deformations has been the calibration of the parameters of the model. Those ones shared with Glen's law, (3) and (4), and its extensions with thermal effects have been set to values suggested in the literature for the predecessor models in the case of alpine glaciers, that is $\mu_0 = 1.5\cdot10^8$, $B = 4610\ K$ and $T_0 = 263\ K$ [15]. From the previous work of Kannan and Rajagopal [12], we get the values $\alpha_1^0 = 10^{16}$ and $k_3 = 0.02$, both ones contributing to the assignment of $\alpha_{KMR,1}$. Then, by supposing that the Arrhenius type thermal dependence acts in the same manner with regard to the viscosity and the normal stress moduli, we have fixed the value of B_1, the activation factor for $\alpha_{KMR,1}$, equal to the value of B, the activation factor for μ_{KMR}, that is $B_1 = B = 4610\ K$.

For the calibration of e we have assumed that the extent of sliding of the mixture of ice and rock and sand grains is related to the value of the relative solid fraction $\bar{\phi}$. So we have fixed $e = e(y)$ as well as a step function with values suitably adjusted at each layer, the bottom 'essentially' rocky zone, the center 'averagely' mixtured zone and the top 'essentially' icy zone (see Fig. 2):

$$e(y) := \begin{cases} e_1 & \text{if } y \in [0, h_1],\ \text{'essentially' rocky zone} \\ e_{12} & \text{if } y \in [h_1, h_2],\ \text{'averagely' mixtured zone} \\ e_2 & \text{if } y \in [h_2, h],\ \text{'essentially' icy zone.} \end{cases} \tag{22}$$

The values of e_1, e_{12}, e_2 and k_1 and k_2, the last parameters to be assigned, have been chosen by a 'trial and error' procedure aimed at shooting the horizontal downslope borehole deformation recorded on 4-4-1989 by Arenson et al. [17], that we estimate by the computed numerical velocity times the elapsed time from observation starting (15-9-1987).

A preliminary mesh refinement test was conducted in order to fix n, the number of subintervals for the finite difference discretization, for getting the highest accuracy of the ODE system approximate solution without loss of significant digits: we found that $n = 2400$ meets the target ($dy = 0.025\ m$).

We shall see that the best fit of the measured profile is obtained with the values $e_1 = 175, e_{12} = 175, e_2 = 1.1$ and $k_1 = 0.015$ and $k_2 = 2$, which identify the purple curves of the most representative results in the figures herein included.

Let us consider, first, the sensitivity of the numerical solution to the value of extent of sliding at the 'averagely' mixtured zone, e_{12}. Actually the effect of p and T, influenced by the reciprocal motion of solid particles within ice, is mostly registered here with the largest change of viscosity occurring for the water release induced by local temperature changes that bring its value above the (eventually decreased) pressure melting point (e_{12} is related to the water content). In Fig. 5 the plot of the computed borehole displacements are drawn for several values of e_{12}. In Fig. 6 the plot of viscosity shows that at altitude $y = h_1$, interface between the 'essentially' rocky zone and the 'averagely' mixtured zone, the larger is the extent of sliding and the smaller becomes the viscosity. This behavior reflects the change of the equilibrium solid fraction that can be observed at Fig. 7: in the transition from the 'essentially' rocky zone to the 'averagely' mixtured zone, the decrease of solid fraction (see $\bar{\phi}$ in Fig. 2) is perceived by the mixture of ice and rock particles as a sudden increase of fluidity, quantified in our model through a sudden decrease of the equilibrium solid fraction, f, and, correspondingly, a sudden decrease of the value of viscosity. This mechanism portrays successfully the sudden internal sliding occurrences (also called shear zone) as it is exhibited in Fig. 5, where each profile shows almost rigid motion of the bottom 'essentially' rocky ice, viscous flow motion of the upper 'essentially' pure ice and, at the intermediate 'averagely' mixtured layer, critical continuously fitting profiles which depend on the value of e_{12}: for $e_{12} = 0.175$ and 1.75 no sudden internal sliding occurs and mixtured ice moves rigidly and smoothly anchored to the 'essentially' rocky ice up to the viscous increase starts at the interface with the 'essentially' icy zone. For $e_{12} \geq 10$ sudden internal sliding occurs with sharper profile as e_{12} gets larger. By comparison with the displacement plot of Arenson et al. observed on 4-4-1989 the purple curve corresponding to $e_{12} = 175$ reports the best match.

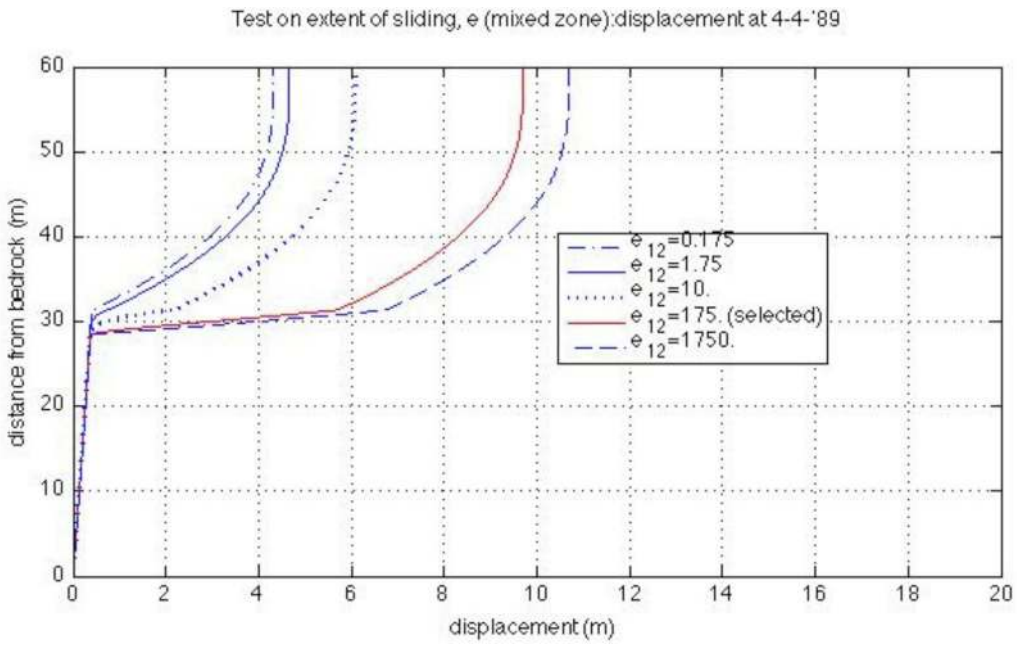

Fig. 5. Numerical borehole displacements at 4-4-1989: sensitivity analysis vs. e_{12}.

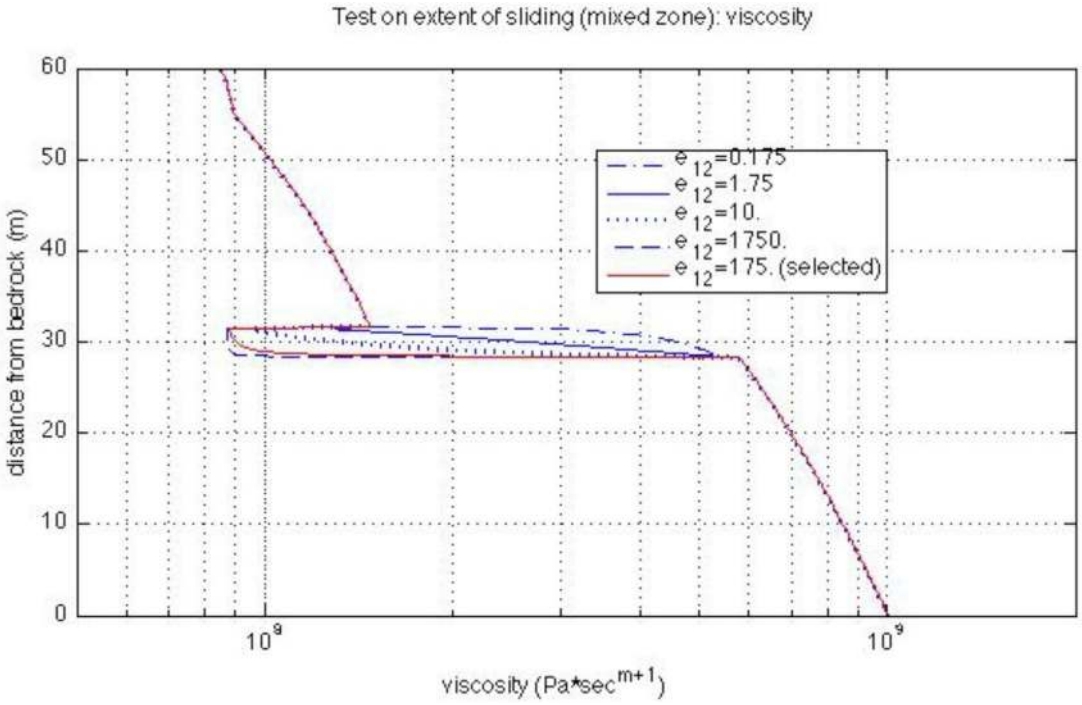

Fig. 6. Numerical viscosity factor, $\mu_{KMR}/[\frac{1}{2}tr(\mathbf{A}_1^2)]^{m/2}$: sensitivity analysis vs. e_{12}.

The sensitivity analysis was concerned with the upper branch of the extent of sliding parametrical function, that is the value e_2. The numerical displacement curves in Fig. 8 show internal sliding occurrence for the three smaller values $e_2 = 0.11, 0.3$ and 1.1 whereas, for $e_2 = 11$ and 110, the profiles exhibit smooth, though steep, viscous growth towards open air. When internal sliding occurs a strong and sudden change of the dynamics of ice establishes, that our model captures just with a significant decrease of value of the extent of sliding parameter (remind $e_{12} = 175$). In our case the physical interpretation of this numerical evidence is that the poor presence of solid grains in the upper 'essentially' icy zone allows just occasional, not effective interaction among solid particles (not enough to induce decrease of viscosity), which contributes to increase the viscosity value, representing an obstacle to free flowing. The graphs of viscosity in Fig. 9 reflect consistently the overall picture. An additional comment on the flection of the viscosity curve few meters beneath ice/atmosphere interface: that is the effect of the Arrhenius exponential function of temperature whose influence in the natural setting shown in Fig. 3 is effective only with sufficiently large values of viscosity.

The sensitivity analysis on the bottom branch of $e = e(y)$, that is on the value e_1, exhibits the fact that when the relative solid fraction, $\bar{\phi}$, is very close to unity the system is not sensitive to changes in e (as the

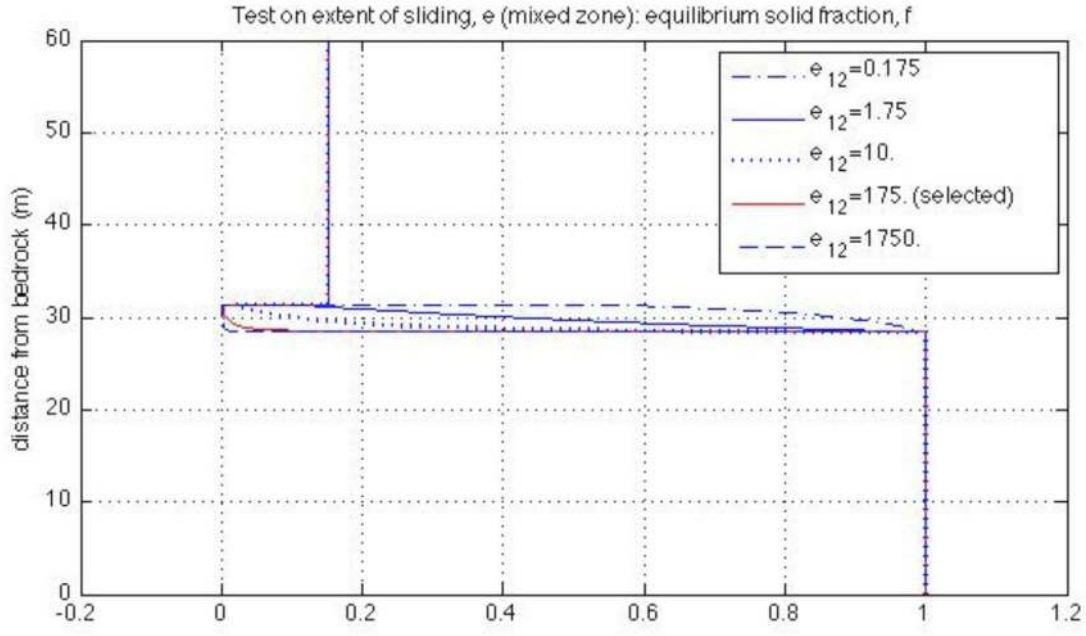

Fig. 7. Equilibrium solid fraction corresponding to solid fraction graph in Fig. 2: sensitivity analysis vs. e_{12}.

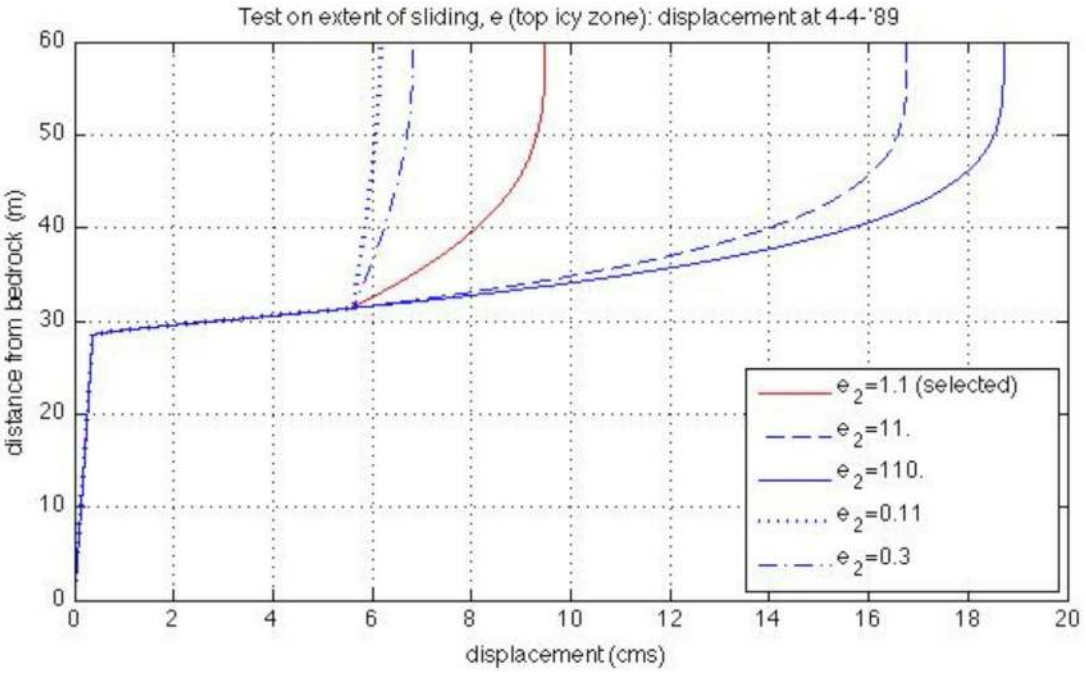

Fig. 8. Numerical borehole displacements at 4-4-1989: sensitivity analysis vs. e_2.

equilibrium solid fraction keeps $f \approx 1$). Fig. 10 represents the evidence that even an unnatural very large value of e_1 induces just a very small change in viscosity with no significant effect on the dynamics. For example, we obtained for $e_1 = 175$, $u(h_1) = 0.243$ cm/yr, $u(h_2) = 3.619$ cm/yr and $u(60m) = 6.139$ cm/yr and for $e_1 = 175\,000$, $u(h_1) = 0.253$ cm/yr, $u(h_2) = 3.637$ cm/yr and $u(60m) = 6.139$ cm/yr.

Finally, the results of the numerical testing on the sensitivity of the system to the parameters k_1 and k_2 are summarized in Figs. 11 and 12 respectively. The formula of viscosity μ_{KMR}(7) assesses how the parameter k_1 influences viscosity where the equilibrium solid fraction is far from unity (top and middle layers). Actually, we see that as k_1 increases, displacement of the essentially icy layer ($f \ll 1$) significantly decreases as for thickening. Furthermore it appears that increasing values of k_2 effectively counteract shearing, in particular within the essentially rocky zone. This characteristic makes this parameter strategical for the purpose of shear zone detection, in addition to e_{12} on which we have already commented. Conversely, decreasing k_2 values induce viscosity lowering and consequent appearance of progressive shear layering from bottom. Let us notice that the influence of changes in the value of parameter k_2, explicitly related in the formula only to lower and more rocky ice, clearly extends to the dynamics of the whole glacier, from bottom upwards, for the lower layers of ice carry along the upper ones laying over.

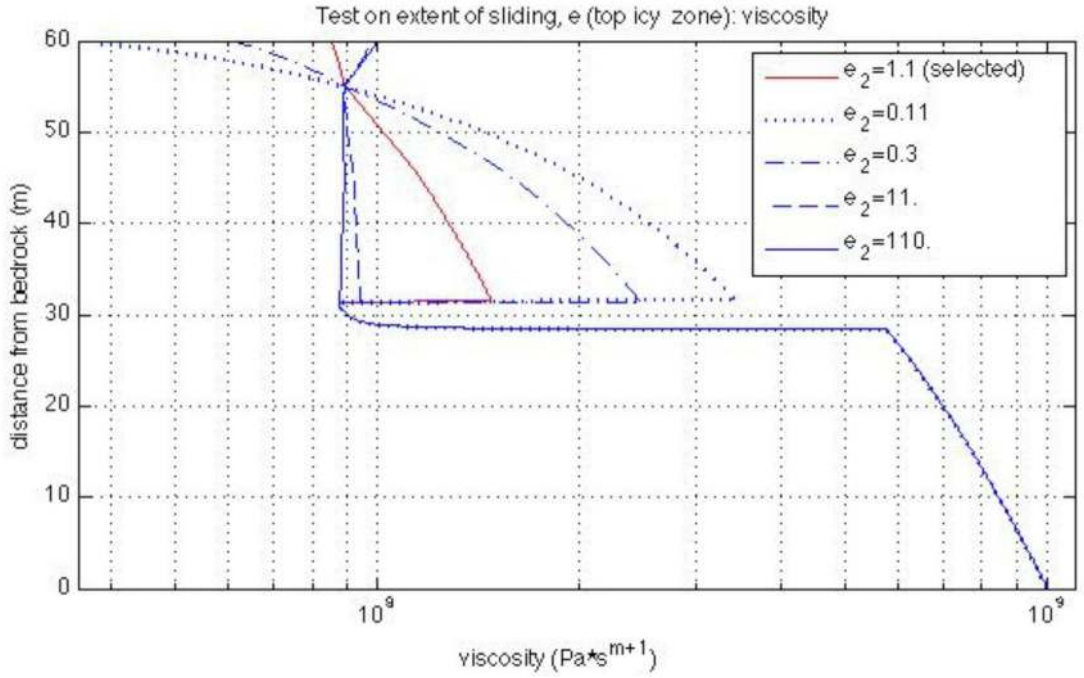

Fig. 9. Numerical viscosity factor, $\mu_{KMR}/[\frac{1}{2}tr(\mathbf{A}_1^2)]^{m/2}$: sensitivity analysis vs. e_2.

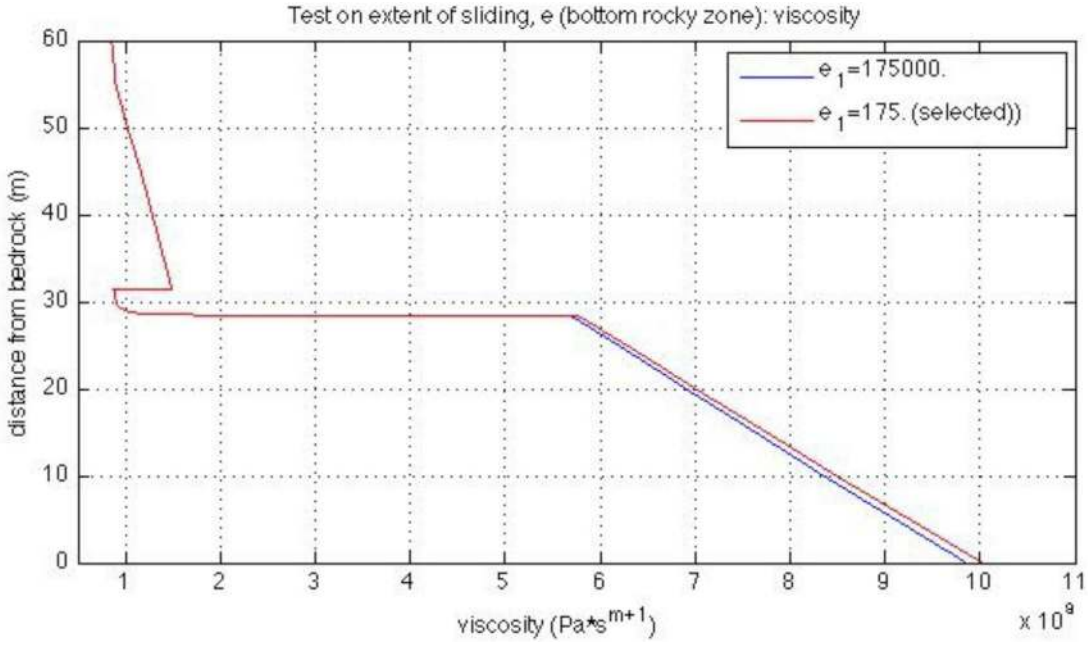

Fig. 10. Numerical viscosity factor, $\mu_{KMR}/[\frac{1}{2}tr(\mathbf{A}_1^2)]^{m/2}$: sensitivity analysis vs. e_1.

3.3. Validation results

With the value of the physical and material parameters previously fixed and the values corresponding to the red curves in the Figs. 5 - 12 we have computed our best approximation of the borehole downslope displacements during the whole time span observed by Arenson et al. in [17]. In Fig. 13 we show the graphs of the obtained numerical results and those of the measured displacements which compare qualitatively very well. In addition we report on the velocity in shear zone, whose measured and computed values amount to 4 cm/yr and 3.9283 cm/yr respectively. Moreover the ratio of the measured shear zone deformation to surface deformation amounts to 59% whereas the ratio of the corresponding numerical deformations results 59.23. Then a relative error of 1.8% and of 0.3% in the reproduction of these two items, respectively, definitely endorse the good match of the numerical and measured curves in Fig. 13 well beyond the qualitative appearance.

Arenson et al. observed that from the start of the measurement campaign, on 5/11/1987, the surface deformation rate kept constant

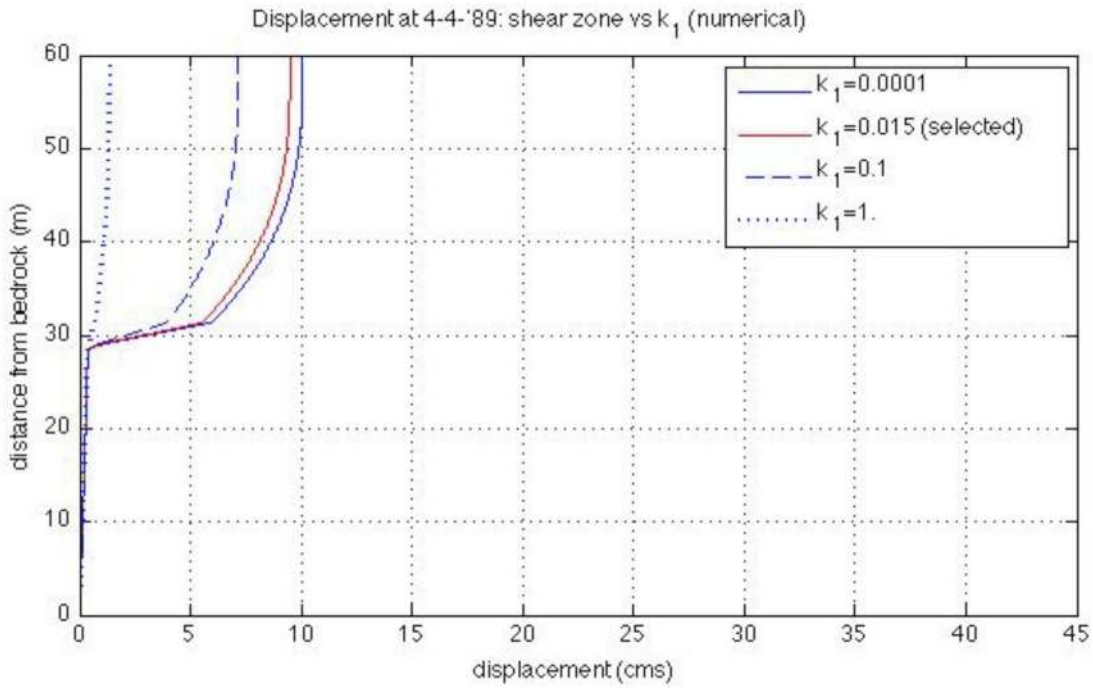

Fig. 11. Numerical borehole displacements at 4-4-1989: sensitivity analysis vs. k_1.

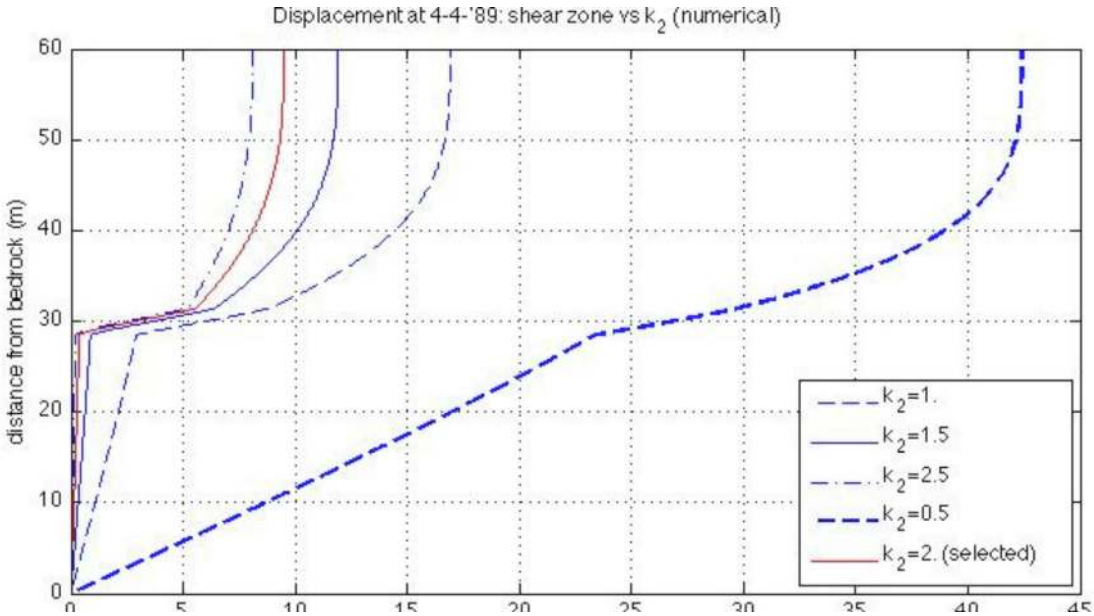

Fig. 12. Numerical borehole displacements at 4-4-1989: sensitivity analysis vs. k_2.

till 1991, then it increased and kept constant till the end of the operations in August 1998 (this is documented in figure 10, a) in [17]). They identified the cause of this change in the increase of about $0.5°C$ of the temperature in the shear zone during the same period, as reported by Vonder Muhll et al. [19]. With the present model which includes temperature effects, we could take into account this change by upgrading the temperature profile (see Fig. 3) and, then, develop the numerical simulation up to the end of the observation time.

The uncertain trend of the measured displacements of the glacier top layer, not captured by the presented simulation, is commented by Arenson et al. as possibly related either to seasonal external temperature changes which do not influence internal ice layers or to distortion effects of the measurement technical equipment. Whatever the cause is, the numerical simulation suggests that the influence of limited changes in the dynamics of the 3 m thick top ice layer upon the underneath one is negligible.

4. Conclusions

In this paper we have provided a validation of the model recently published in [1] for the numerical description of non-isothermal rock-glacier flows. We have based this study on the reproduction of the borehole downslope displacements of the Alpine rock glacier, Murtel-Corvatsch, in Switzerland, as well as documented by Arenson et al. in [17]. This case appears particularly suitable to our purpose because it exhibits internal sliding occurrence in correspondence of an averagely

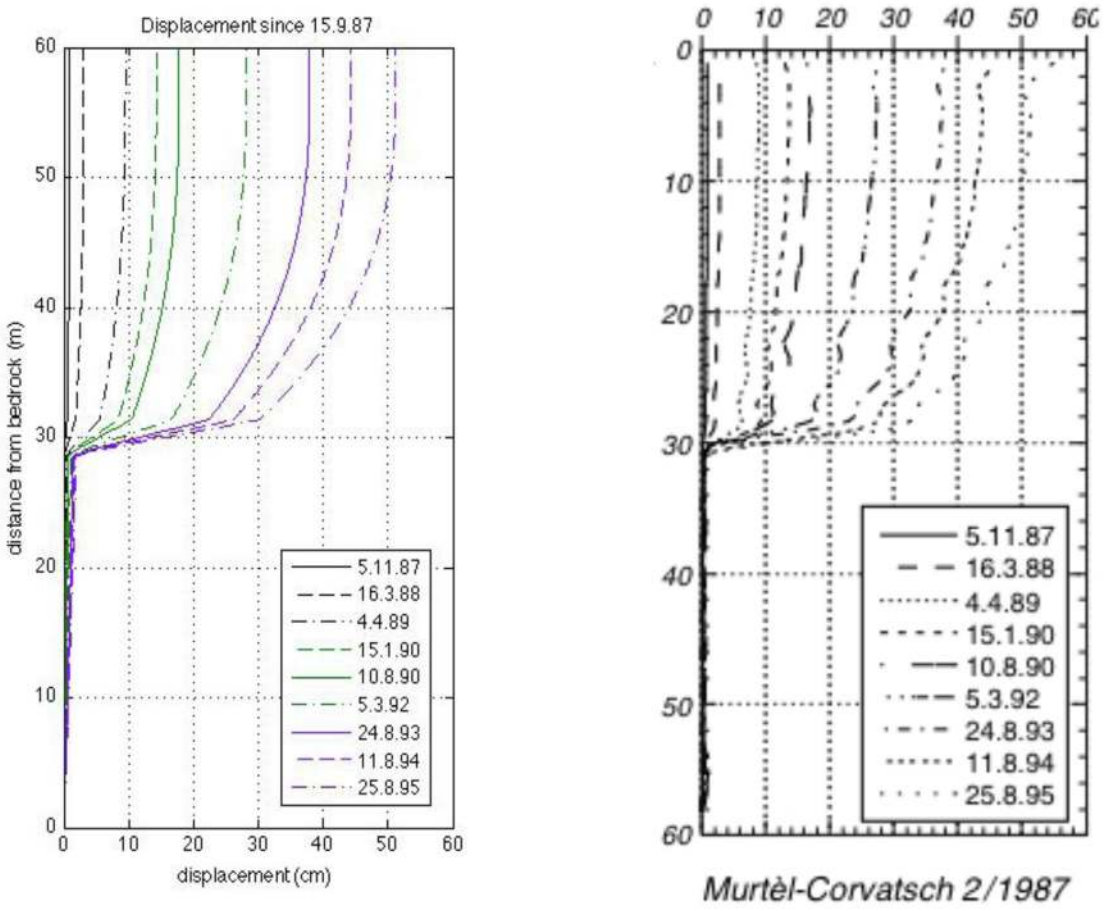

Fig. 13. Borehole downslope displacements: numerical (left) vs measured by Arenson et al. (see Figure 9, a) in [17]) (right).

mixtured zone with ice and solid particles and sand grains, a typical and critical condition which makes rock glaciers potentially very dangerous for human settlements. It allowed also to test the ability of the model to describe the impact of a temperature field change within the glacier as, at mid-term of the observation time period, 1987–1995, on-field measurements pointed out an increase of the displacement rate attributed to an increase of $0.5°C$ of the temperature at the shear zone. This event is characteristic of the shear zone as the relatively rapid movement of ice and rocky particles and the consequent friction typically induce mechanical dissipation and internal heating.

After the sensitivity study of the model parameters linked to the described natural set-up evolution (e.g. e_1, e_{12}, e_2, k_1 and k_2 in (7), (10) and (22)), whose change impact has been discussed in detail, the numerical results obtained with the parameters selected values are qualitatively and quantitatively impressive as it is shown in Fig. 13, where the present numerical computations and Arensons et al.'s measured displacement profiles are compared.

The proposed model appears eligible for extensive use in computational glaciology. However for future modeling tasks of rock-glacier flows, we stress the importance of having on-field measured data from paradigmatic set-ups which allow the calibration of the sensible parameters in relation to the specific ice and rock and sand grains mixture composition.

Declaration of competing interest

The authors declare that they have no known competing financial interests or personal relationships that could have appeared to influence the work reported in this paper.

Acknowledgments

Authors acknowledge Piano Nazionale Ricerca Antartide (PNRA), the funding agency of the project PNRA16-00121 ENIGMA which the present research is part of. K.R.R. thanks the Office of Naval Research for its support.

D.M. acknowledges the licence n. 5016591052717 released by Wiley for reuse of Figure 9.a in [17] as right part of Figure 13 in present article.

References

[1] K. Kannan, D. Mansutti, K.R. Rajagopal, S. Urbini, Mathematical modeling of rock glacier flow with temperature effects, in: P. Cannarsa, D. Mansutti, A. Provenzale (Eds.), Mathematical Approach to Climate Change and Its Impacts, in: Springer-INDAM Series, vol. 38, 2020, pp. 137–148.

[2] J.W. Glen, The creep of polycrystalline ice, Proc. R. Soc. Lond. Ser. A Math. Phys. Eng. Sci. 228 (1175) (1955) 519–539.

[3] D.F. McTigue, S.L. Passman, S.J. Jones, Normal stress effects in the creep of ice, J. Glaciol. 31 (108) (1985) 120–126.

[4] W.R. Schowalter, Mechanics of Non-Newtonian Fluids, Pergamon Press, London, 1978.

[5] J.E. Dunn, K.R. Rajagopal, Fluids of differential type: critical review and thermodynamical analysis, Intl. J. Eng. Sci. 33 (1995) 689–729.

[6] C.-S. Man, Q.-S. Sun, On the significance of normal stress effects in the flow of glaciers, J. Glaciol. 33 (115) (1987) 268–273.

[7] P.D. Barrette, I.J. Jordan, Pressure-temperature effects on the compressive behavior of laboratory-grown and iceberg ice, Cold Reg. Sci. Technol. 36 (2003) 25–36.

[8] M. Arcangioli, A. Farina, L. Fusi, G. Saccomandi, Constitutive equations with pressure-dependent rheological parameters for describing ice creep, J. Glaciol. 65 (252) (2019) 557–564.

[9] P. Duval, The role of the water content on the creep rate of polycrystalline ice, IAHS Publ. 118 (1997) 29–33.

[10] P.L. Moore, Deformation of debris-ice mixtures, Rev. Geophys. 52 (2014) 435–467.
[11] W. Lawson, C. Elliott, Strain rate effects on the strength of debris-laden glacier ice, N. Z. J. Geol. Geophys. 46 (2010) 323–330.
[12] K. Kannan, K.R. Rajagopal, A model for the flow of rock glaciers, Int. J. Non-Linear Mech. 48 (2013) 59–64.
[13] P. Mills, P. Snabre, Apparent viscosity and particle pressure of a concentrated suspension of non-brownian hard spheres near the jamming transition, Eur. Phys. J. E 30 (3) (2009) 309–316.
[14] J.F. Morris, F. Boulay, Curvilinear flows of noncolloidal suspensions: the role of normal stresses, J. Rheol. 43 (1999) 1213–1237.
[15] K.M. Cuffey, W.S.B. Paterson, The Physics of Glaciers, BH Elsevier, Croydon, UK, 2010.
[16] J.E. Dunn, R.L. Fosdick, Thermodynamics, stability and boundedness of fluids of complexity 2 and fluids of second grade, Arch. Ration. Mech. Anal. 56 (1974) 192–252.
[17] L. Arenson, M. Hoeltzle, S. Springman, Borehole deformation measurements and internal structure of some rock glaciers in Switzerland, Permafr. Periglac. Process. 13 (2002) 117–135.
[18] G. Ovralez, F. Bertrand, S. Rodts, Local determination of the constitutive law of a dense suspension of non-colloidal particles through magnetic resonance imaging, J. Rheol. 50 (2006) 259–292.
[19] D. Vonder Muhll, T. Stucki, W. Haeberli, Borehole temperatures in alpine permafrost: a ten year series, in: Proceedings of the 7th International Conference on Permafrost, Yellowknife, Nordicana 57, Universite' Laud, 1998, pp. 1089–1095.